J. Fluid Mech. (2011), *vol.* 666, *pp.* 477–505.
doi:10.1017/S0022112010004301

The steady-state form of large-amplitude internal solitary waves

STUART E. KING†, MAGDA CARR AND DAVID G. DRITSCHEL

School of Mathematics and Statistics, University of St Andrews, Fife KY16 9SS, UK

(Received 29 January 2010; revised 5 August 2010; accepted 11 August 2010; first published online 10 November 2010)

A new numerical scheme for obtaining the steady-state form of an internal solitary wave of large amplitude is presented. A stratified inviscid two-dimensional fluid under the Boussinesq approximation flowing between horizontal rigid boundaries is considered. The stratification is stable, and buoyancy is continuously differentiable throughout the domain of the flow. Solutions are obtained by tracing the buoyancy frequency along streamlines from the undisturbed far field. From this the vorticity field can be constructed and the streamfunction may then be obtained by inversion of Laplace's operator. The scheme is presented as an iterative solver, where the inversion of Laplace's operator is performed spectrally. The solutions agree well with previous results for stratification in which the buoyancy frequency is a discontinuous function. The new numerical scheme allows significantly larger amplitude waves to be computed than have been presented before and it is shown that waves with Richardson numbers as low as 0.062 can be computed straightforwardly. The method is also extended to deal in a novel way with closed streamlines when they occur in the domain. The new solutions are tested in independent fully nonlinear time-dependent simulations and are verified to be steady. Waves with regions of recirculation are also discussed.

Key words: internal waves, solitary waves, stratified flows

1. Introduction

Internal solitary waves (ISWs) are understood to be an ubiquitous feature of coastal ocean areas (Ostrovsky & Stepanyants 1989; Stanton & Ostrovsky 1998; Moum *et al.* 2003; Helfrich & Melville 2006). They are frequently observed to have large amplitudes, that is, with maximal pycnocline displacements several times the undisturbed depth of the pycnocline (Stanton & Ostrovsky 1998). At such amplitudes the waves are highly nonlinear and differ markedly from the predictions of well-known weakly nonlinear Korteweg–de-Vries (KdV) theory (see Miles 1980).

The propagation characteristics of large-amplitude ISWs are important since they transport mass and energy in coastal oceans. In addition, the interaction of these waves with underwater structures, particularly those associated with oil and gas extraction, may have implications for the design of such structures. Furthermore, shoaling and breaking of ISWs may cause significant mixing in the water column (Grue *et al.* 2000; Fructus *et al.* 2009), and hence redistribution of available potential energy. Therefore,

† Email address for correspondence: stuart@mcs.st-and.ac.uk

an understanding of the steady-state form of ISWs at large amplitudes is important to the fundamental understanding of such problems.

Oceanic ISWs may occur in situations, where the background conditions vary significantly. For example, the water depth can change as a wave shoals or moves into deeper water and stratification can change with season or location. In the current approach, waves moving in a constant depth of water with a constant background stratification and no background shear are considered (a short discussion of how a net shear may be added is given in § 2). The idealized assumptions are a consequence of studying steady-state wave behaviour, since waves moving in non-constant conditions will be inherently unsteady. In addition, a rigid horizontal lid is employed and the lower boundary is assumed to be horizontal and flat. Free slip conditions are used on both top and bottom boundaries. Hence, free surface and frictional effects are neglected. These boundary conditions simplify the mathematics and are widely employed when studying problems of this nature (see e.g. Turkington, Eydeland & Wang 1991; Brown & Christie 1998; Choi & Camassa 1999; Fructus & Grue 2004). In the ocean, waves often occur in rank ordered groups, but it is well known that large-amplitude internal waves have greater wave speeds than their smaller counterparts and so the individual waves tend to separate as time evolves (Ostrovsky & Stepanyants 1989). Hence, consideration of a solitary wave is thought to be appropriate here.

Previous approaches to the problem of finding the steady-state form of ISWs in a system with a given stratification have focused largely on using the Dubreil-Jacotin–Long (DJL) equation as a means of analysing the fluid flow. In particular, various authors have considered layered profiles with either constant density or constant stratification in each layer (Grue *et al.* 2000; Fructus & Grue 2004), while others have considered smooth profiles of stratification (Turkington *et al.* 1991; Brown & Christie 1998; Lamb 2002). Different methods are appropriate for different stratifications. For constant density layers, solving Laplace's equation for the streamfunction in each layer and matching across layer boundaries is sufficient (Funakoshi & Oikawa 1986; Grue *et al.* 1999; Rusås & Grue 2002). Alternatively, it is possible to run a fully nonlinear time dependent simulation long enough to converge on the steady state (Vlasenko, Brandt & Rubino 2000).

In the present paper, a new derivation of a useful variant of the DJL equation is presented in terms of the streamfunction and buoyancy which are natural variables to consider in an incompressible Boussinesq fluid system. A new procedure for finding fully nonlinear ISW solutions for a background buoyancy (likewise density) stratification that is sufficiently smooth is also given. This procedure is much simpler than the integral methods described in Fructus & Grue (2004) and requires no matching across layers. It also represents an alternative approach to the method presented by Turkington *et al.* (1991). This method obtains solutions for ISWs in a smooth background stratification, but substitutes a variational problem for the direct problem solved here. To reproduce a similar layered structure to Fructus & Grue (2004), the profile of the stratification (expressed through buoyancy frequency $N(Y)$, where Y is a mass coordinate) is smoothed across layers. It is shown that it is possible to match the results from a sharply layered stratification acceptably well by comparing results to those provided by Fructus & Grue (2004). Other methods for obtaining solutions describing large-amplitude ISWs often have difficulty in finding waves with small values of the Richardson number. In particular, Lamb (2002) (the methodology of which follows that of Turkington *et al.* 1991) describes several limits which restrict the amplitude at which solutions can be found. Two of these limits can be regarded as shortcomings of the model of Turkington *et al.* (1991) and are

worth addressing since that methodology is the main means at present of obtaining large-amplitude ISW solutions for a smooth background stratification. The limits are (i) that solutions describing waves with Richardson number much below 0.25 cannot be found (ii) that waves with closed streamlines which lead to a stable wave cannot be found. In the numerical scheme presented here the Richardson number is not a limiting factor and ISW solutions are found with minimum Richardson numbers in the pycnocline as low as 0.062. In particular waves with Richardson number well below 0.25 are straightforwardly computed, as documented in § 3. Although representing a theoretical steady state, they are not expected to be stable if they are evolved in time, as it is known that large waves with small Richardson number can exhibit a Kelvin–Helmholtz type instability as documented experimentally by Fructus *et al.* (2009).

Previous authors have suggested closed streamlines may occur when the buoyancy frequency is non-zero at the top/bottom of the domain for a wave of depression/elevation (Brown & Christie 1998; Fructus & Grue 2004). Such methods, however, are expected to be unstable since density is unstably stratified in the closed streamline region. A new approach is proposed here for obtaining the density (or buoyancy) in areas in which closed streamlines occur, and where no large-scale recirculation exists in the steady-state flow. The new solutions presented suppose instead that a region of the flow is essentially stagnant in the frame of reference moving with the wave. The area of the stagnant region simply increases as the amplitude of the wave increases.

Lamb (2002) also comments that a conjugate flow limit exists in which waves become flat at the centre and longer as wave amplitude increases (Benjamin 1966; Lamb & Wan 1998). This is also observed in the solutions presented here. Note that this is not a shortcoming of the method presented by Turkington *et al.* (1991), or the numerical scheme presented here as waves can continue to be found even as they flatten in the centre. As the wave amplitude increases a set of solutions is obtained for which the front and back of the wave become further apart and the two fronts move like two smooth bores. This phenomenon has been noted previously in the literature (see e.g. Lamb & Wan 1998), and is a real physical limitation of the system.

2. Description of the methodology

A computational domain is chosen so that a wave is centred in the domain pictured in figure 1. The domain is periodic in the horizontal direction x and of length 2π. This ensures that the use of fast Fourier transforms is possible in x. In the vertical direction y, the flow is bounded between a rigid free-slip horizontal floor at $y=0$ and a rigid free-slip lid at $y=L_y$. In the vertical direction either Fourier sine or cosine transforms are used to represent fields depending on whether a given field is zero at the domain edges, in which case sines are used, or its derivative is zero, in which case cosines are used. The domain is set-up by specifying the domain aspect ratio which is then used to set L_y (since the domain length in the x-direction is fixed at 2π). Using a small aspect ratio ($L_y/2\pi=0.05$ throughout the paper) ensures that the domain is long compared to the length of the waves. Although no non-dimensionalization is performed it is clear that many flows may be in some sense similar. In particular, the domain height can be re-scaled so that any flow with a layered structure in which the layers occur at the same relative positions, but in a different overall depth, can be considered as similar. Similarly time can be re-scaled so that any one value of the buoyancy frequency N^2 can be re-scaled so that $N^2=1$ and the flow will remain similar. Commonly this is taken so that either an average or a maximum value of

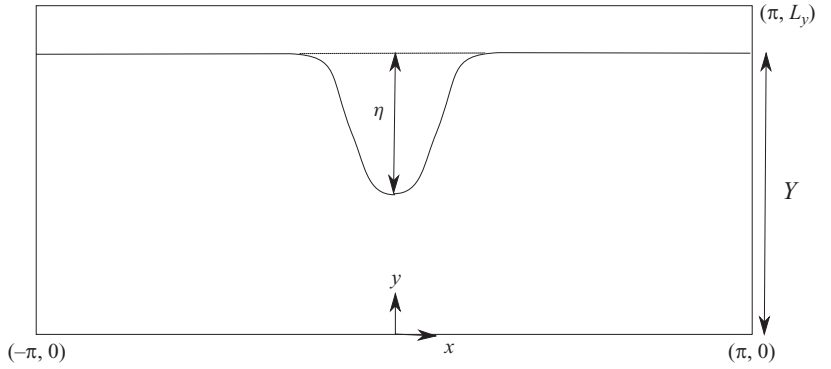

FIGURE 1. Schematic diagram showing the computational domain, in a frame of reference following a wave at a calculated wave speed, c. The diagram shows the generic path of a streamline in this frame. The streamline has a deflection in the centre of the domain due to the wave and has an undisturbed height upstream and downstream of the wave.

N^2 is set to one. In the following sections, when dealing with a layered stratification, stratifications are considered in which the middle layer (or top layer for a two layer stratification) has $N^2 = 1$. Through a re-scaling of time, results for these particular stratifications are applicable to a wider class of stratifications.

The relevant equations used to model the flow are the inviscid, incompressible Oberbeck–Boussinesq equations in two dimensions:

$$\rho_0 (\boldsymbol{u}_t + \boldsymbol{u} \cdot \nabla \boldsymbol{u}) = -\nabla p - \rho g \boldsymbol{j}, \tag{2.1}$$

$$\rho_t + \boldsymbol{u} \cdot \nabla \rho = 0, \tag{2.2}$$

$$\nabla \cdot \boldsymbol{u} = 0, \tag{2.3}$$

where ρ_0 is a convenient constant reference density, $\boldsymbol{u} = (u, v)$ is the fluid velocity vector, t denotes time, $\nabla = (\partial/\partial x, \partial/\partial y)$ is the gradient operator, p is the fluid pressure, ρ is the fluid density, g is the gravitational acceleration constant and $\boldsymbol{j}$ is the vertical unit vector. Introducing a buoyancy variable such that $b = -g(\rho - \rho_0)/\rho_0$, and re-scaling pressure in a suitable way transforms (2.1)–(2.3) to equations which only involve buoyancy directly and not density

$$\boldsymbol{u}_t + \boldsymbol{u} \cdot \nabla \boldsymbol{u} = -\nabla p + b \boldsymbol{j}, \tag{2.4}$$

$$b_t + \boldsymbol{u} \cdot \nabla b = 0, \tag{2.5}$$

$$\nabla \cdot \boldsymbol{u} = 0. \tag{2.6}$$

Note that the computational domain is chosen so that in a frame of reference that moves at the wave speed, c, streamlines are generically of the form shown in figure 1. That is they have a point on the right-hand edge of the domain which has zero displacement height (defined as $y = Y$). This, along with ensuring that streamlines approach the edges of the domain with zero gradient, ensures that the wave is truly solitary and is unaffected by interactions with identical waves in the periodic boxes in front and behind the periodic domain being considered. Such a scheme clearly relies on being able to draw a streamline from any point within the domain to the upstream edge of the domain. This is problematic in cases where closed streamlines are present in the flow, and indeed such flows are known to be relevant to large-amplitude ISWs (Grue *et al.* 2000; Carr *et al.* 2008). A new procedure for dealing with closed streamlines will be discussed in § 2.1 below.

A streamfunction $\psi(x, y)$ in the fixed frame is introduced, such that in a fixed frame $v = \psi_x$ and $u = -\psi_y$. Furthermore, a streamfunction $\widetilde{\psi}(x, y)$ in the frame moving with the wave speed c is introduced. The fixed and moving frame streamfunctions are related by

$$\widetilde{\psi}(x, y) = \psi(x, y) + cy. \tag{2.7}$$

It follows that $\widetilde{u} = u - c$ and $\widetilde{v} = v$. For flows with no closed streamlines in the moving frame it is then possible to write

$$\widetilde{\psi}(\pi, Y) = \widetilde{\psi}(x, y), \tag{2.8}$$

where Y denotes the height of the streamline through the point (x, y) at the upstream (right-hand) edge of the domain. Re-writing (2.8) and utilizing (2.7) gives

$$\begin{aligned} \psi(\pi, Y) + cY &= \psi(x, y) + cy, \\ &= \psi(x, y) + c(Y - \eta), \end{aligned} \tag{2.9}$$

where $\eta(x, y) = Y - y$ is the streamline displacement at any general point in the domain (η is defined to be positive for downwards displacements). Note that ψ may be chosen so that $\psi(\pi, Y) = 0$ since in the stationary frame velocities far from the centre of the wave are zero. Therefore, from (2.9) it can be deduced that

$$\eta(x, y) = \frac{\psi(x, y)}{c}. \tag{2.10}$$

Reversing this logic, a height Y can be defined for any point (x, y) in the domain such that the streamline through that point reaches a height Y at the upstream domain edge. Therefore, it follows that

$$Y = y + \eta = y + \frac{\psi(x, y)}{c}. \tag{2.11}$$

This is useful in that if a quantity $A(x, y)$ is materially conserved then the value of that quantity can be found throughout the domain simply from the value at the domain edge: $A(x, y) = A(\pi, Y)$. Since the values of all fields reduce to their background states at the domain edge (i.e. velocities are zero, the density takes background values and pressure is hydrostatic), this presents a useful method to simplify the problem of finding field values throughout the domain.

This model can be generalized to include the effects of a net shear across the water column. A profile of horizontal velocity (and hence streamfunction) can be specified at the domain edge. This would ensure that the background has some profile of horizontal velocity to describe the shear far away from the wave. Then the difference in perturbation streamfunction values between the top and bottom of the domain specifies a net shear across the domain. In this paper no consideration is given to this problem. A fuller exploration of solutions with a background shear is left as the subject of future work (see also Stastna & Lamb 2002; Lamb 2003).

Expressing (2.4)–(2.6) in terms of the streamfunction in the moving frame $\widetilde{\psi}(x, y)$, a steady flow in the moving frame must satisfy

$$J(\widetilde{\psi}, u) = -p_x, \tag{2.12}$$

$$J(\widetilde{\psi}, v) = -p_y + b, \tag{2.13}$$

$$J(\widetilde{\psi}, b) = 0, \tag{2.14}$$

where $J(A, B) = A_x B_y - A_y B_x$ denotes the Jacobian. Note that at the domain edge (2.12) and (2.13) reduce to $p = \bar{p}(Y)$ and $\bar{p}_Y = \bar{b}(Y)$, respectively, where barred variables

denote the background (undisturbed) buoyancy and pressure. Buoyancy frequency $N(Y)$ is introduced and defined by

$$N^2(Y) = \bar{b}_Y = -\frac{g}{\rho_0}\frac{\partial \bar{\rho}}{\partial Y}. \tag{2.15}$$

The condition that a field $A(x, y)$ is materially conserved, $(\widetilde{\boldsymbol{u}} \cdot \nabla)A = 0$, simply reduces to the condition that $J(\widetilde{\psi}, A) = 0$ in this notation. It can be seen immediately from (2.14) that buoyancy is a materially conserved field. Another field having this property is the Bernoulli pressure $P(x, y)$, defined as

$$P = p + \tfrac{1}{2}(u - c)^2 + \tfrac{1}{2}v^2 - \tfrac{1}{2}c^2 - yb. \tag{2.16}$$

The procedure outlined by Yih (1960) and Grue *et al.* (2000) can be followed to obtain an equation of Helmholtz form for vorticity (the equivalent of Yih 1960, Eq. (10); Benjamin 1966, Eq. (2.13); Grue *et al.* 2000, Eq. (3.1)), namely

$$\zeta = \nabla^2\psi = \frac{\mathrm{d}P}{\mathrm{d}\widetilde{\psi}} + y\frac{\mathrm{d}b}{\mathrm{d}\widetilde{\psi}}. \tag{2.17}$$

This is a slightly simplified version of the DJL equation (Dubreil-Jacotin 1932; Long 1953). Since both P and b are conserved along streamlines it is possible to use the domain edge values to evaluate the derivatives in (2.17), so that

$$\frac{\mathrm{d}P}{\mathrm{d}\widetilde{\psi}} = \frac{\mathrm{d}\bar{P}}{\mathrm{d}\widetilde{\psi}} = \frac{1}{c}\bar{P}_Y \quad \text{and} \quad \frac{\mathrm{d}b}{\mathrm{d}\widetilde{\psi}} = \frac{\mathrm{d}\bar{b}}{\mathrm{d}\widetilde{\psi}} = \frac{1}{c}\bar{b}_Y = \frac{N^2(Y)}{c}, \tag{2.18}$$

by use of (2.15) and noting that $\mathrm{d}\widetilde{\psi}/\mathrm{d}Y = c$ since from (2.7) and (2.11) $\widetilde{\psi} = cY$ throughout the domain. Expanding the Bernoulli pressure derivative using (2.16) gives

$$\frac{\mathrm{d}\bar{P}}{\mathrm{d}\widetilde{\psi}} = \frac{1}{c}\frac{\mathrm{d}}{\mathrm{d}Y}(\bar{p} - Y\bar{b}) = -\frac{1}{c}Y\bar{b}_Y = -\frac{Y}{c}N^2(Y), \tag{2.19}$$

recalling $\bar{p}_Y = \bar{b}$. Therefore, (2.17) can be written as

$$\zeta = (y - Y)\frac{N^2(Y)}{c}. \tag{2.20}$$

Finally, using (2.11) gives

$$\zeta = \nabla^2\psi = -\frac{N^2(Y)}{c^2}\psi. \tag{2.21}$$

Note that (2.21) involves $N^2(Y)$ and not simply $N^2(y)$, making the equation explicitly nonlinear since Y itself depends on ψ. Equation (2.21) has been widely used in the context of ISWs (Davis & Acrivos 1967; Brown & Christie 1998; Lamb & Wan 1998; Lamb 2002). The procedure for obtaining the fully nonlinear solutions to this equation is given in § 2.2, while details of the linear and weakly nonlinear solutions to the problem are given in the Appendix.

2.1. *Closed streamline regions*

It is known that in domains where the value of N^2 does not go to zero at either the top or the bottom of the domain (for waves of depression or elevation, respectively) closed streamlines can occur (Brown & Christie 1998; Fructus & Grue 2004). This immediately presents a problem for the above method, since in a closed streamline region the height, Y defined by $Y = y + \psi/c$, cannot be interpreted as an actual

streamline height at the upstream edge of the domain. Instead if the definition of Y is extended to be the notional height of the streamline upstream, then it is possible to continue. For closed streamlines, the height Y defined in this way simply lies outside the domain $[0, L_y]$. Therefore, it is necessary to consider how the values of $N^2(Y)$ and $\bar{b}(Y)$ should be extended to allow for values outside the domain. Fructus & Grue (2004) have previously considered waves of depression, while Brown & Christie (1998) have considered both waves of depression and elevation. Both sets of authors allowed the function for $N^2(Y)$, (or equivalently $F'(\psi)$ in Brown & Christie 1998) to be continued by simply extending the domain of definition of the function, but keeping the same functional form (an idea that goes back to Davis & Acrivos 1967). In a region of constant N^2 as in Fructus & Grue (2004), this would correspond to

$$N^2(Y) = N^2(L_y), \quad \text{for} \quad Y > L_y. \tag{2.22}$$

Such a definition, however, leads to an area of the flow containing a buoyancy field that is statically unstable (both Brown & Christie 1998 and Fructus & Grue 2004 noted this). A flow defined in this way cannot be stable and therefore solutions containing regions of closed streamlines of this sort cannot represent realistic steady-state descriptions of ISWs.

The subject of recirculating vortex cores in ISWs has been considered in the weakly nonlinear regime by Derzho & Grimshaw (1997), Aigner, Broutman & Grimshaw (1999) and in a more unusual flow regime by Derzho & Grimshaw (2002). Each of these consider a constant density recirculating core of fluid and Derzho & Grimshaw (1997) make a convincing argument for why this must in fact be the only stable configuration. They also refer to the results of Grimshaw (1969), which are analogous to the Batchelor–Prandtl theorem, but for a fluid with non-constant density. Grimshaw (1969) argues that in the presence of a small amount of diffusion (both of momentum and density in the form of heat or salinity diffusion) then a two-dimensional flow with nested streamlines must tend to a constant density and vorticity. Both values of buoyancy and vorticity must then be determined by the boundary of the closed region, since (2.21) is not strictly valid in this region. This would appear to settle any argument as to the structure of a closed recirculating core in an ISW. Care should be taken in applying this theory though since it requires that there be sufficient time for diffusion to act, which could be problematic at the very large Reynolds numbers characteristic of real oceanic ISWs.

As further evidence that a constant buoyancy core is the only stable configuration, there are various observations of waves for which a constant density recirculating core is seen. In particular, the observations of Clarke, Smith & Reid (1981), Doviak & Christie (1989), Cheung & Little (1990) and Doviak, Chen & Christie (1991) of atmospheric solitary waves or bores, all describe recirculating regions with constant (or nearly constant) density which is equal, or just greater than, that at the surface upstream. A similar picture is seen in an oceanic setting at least for elevation waves. For example, Scotti & Pineda (2004) have observed constant density trapped cores of fluid. Also in laboratory experiments Manasseh, Ching & Fernando (1998) have observed solitary waves with trapped constant density cores, although in this case the core could be due to the generation mechanisms used in the experiments. In addition Grue *et al.* (2000) and Carr *et al.* (2008) observed waves with trapped cores, but no density measurements were made so it is unclear whether the density was constant in the core in these cases. Additionally the vorticity measured in these experiments was found to include small weaker vortices within the core, although these could be due to the generation mechanism of the experiments, and may be transitory (transitory

instabilities of the vortex core can be long-lived, see the constant density, non-zero vorticity core discussed later in § 3). Constant density cores were also found in the unsteady simulations of lock release flows in a stratified fluid presented by White & Helfrich (2008).

The conclusion of these observations leads to the contention here that a better choice for extending the function $N^2(Y)$ might be $N^2(Y) = 0$ for $Y > L_y$ as opposed to $N^2(Y) = N^2(L_y)$. In practice, however, a sharp but continuous transition to this value is allowed as follows:

$$N^2(Y) = N^2(L_y)\exp\left(-((Y - L_y)/W)^2\right), \quad \text{for} \quad Y > L_y, \tag{2.23}$$

where W is a small adjustment length scale. The scale W is chosen so that $W \ll L_y$, in order to minimize the area in which static instability occurs.

Then it remains to determine the flow pattern within any closed streamline region. The simplest approach to this problem is to assume the continued validity of (2.21) and so obtain vorticity values directly from the values of $N^2(Y)$ given above in (2.22) and (2.23). This is the approach used in both Brown & Christie (1998) and Fructus & Grue (2004). However, as they also note (2.21) is not strictly valid in this region; nevertheless, results from the use of both (2.22) and (2.23) are discussed in § 3. Steady-state solutions in each case are presented along with an examination of the stability of those solutions in unsteady numerical simulations of (2.4)–(2.6). An alternative approach is to model the flow within the core using a vorticity-streamfunction relation and match it to the flow outside the core through a pressure continuity condition at the core boundary. Derzho & Grimshaw (1997) did this for a linear background stratification, and recently this approach has been extended for arbitrary stratifications (Helfrich & White 2010).

The simplest solutions possible for flow within the closed streamline region are for the region to have constant vorticity. Since this vorticity must be set by the bounding streamline to the closed region two possibilities present themselves, which are analogous to the continuation of buoyancy in the argument above. Either vorticity, like $N^2(Y)$, can drop to zero over some small distance, W, or the value of vorticity can be set by the value of the term $\mathrm{d}P/\mathrm{d}\widetilde{\psi}$ from (2.17) at the edge of the closed streamline region. Note that there is a jump discontinuity in the term $\mathrm{d}b/\mathrm{d}\widetilde{\psi}$ at exactly this point in the stratification, however, taking the limit from above shows that the contribution from this term is zero. The first of these scenarios gives essentially a zero vorticity core of fluid and is equivalent to the previously discussed case of simply using (2.21) and (2.23) to obtain a smooth transition into the core. The second option leaves open the possibility of a rotating core with some vorticity whose value can once again be determined from upstream conditions (since the bounding streamline will be the last to connect upstream), in which case

$$\zeta_{core} = \frac{\mathrm{d}\bar{P}}{\mathrm{d}\widetilde{\psi}}(L_y) = -\frac{L_y N^2(L_y)}{c}, \tag{2.24}$$

where ζ_{core} denotes the constant vorticity in the closed streamline region. Note that this prescription for ζ_{core} does not rely on the Batchelor–Prandtl diffusion argument used by Grimshaw (1969). This possibility is also presented and discussed in § 3, where both steady-state solutions and unsteady simulations are presented. Solutions with more elaborate distributions of vorticity within a constant density core are perhaps possible but are left for future study. The argument presented in § 3 concerning the stability of a constant vorticity core can easily be generalized to apply to a rotating

core with any (non-zero) distribution of vorticity. It should be noted once again that the observations from experiments involving ISWs with trapped cores (Grue *et al.* 2000; Carr *et al.* 2008) have not shown a constant or zero vorticity core, but often have a region with weak smaller vortices contained within it. Resolving this issue is the subject of further research into the unsteady behaviour and breaking of ISWs.

2.2. *Computational implementation*

To compute solutions of (2.21) for a given $N^2(Y)$ the following iterative procedure is carried out. First a uniform computational grid is set-up within the domain described in figure 1, with n_x intervals in x and n_y intervals in y. The background buoyancy field $\bar{b}(Y)$ is found by integrating the specified profile of $N^2(Y)$ with respect to Y ($\bar{b}(0)=0$ can be used without loss of generality). The iterative solution procedure is then started with a guess for ψ, here the weakly nonlinear solitary wave solution as outlined in Fructus & Grue (2004), for instance (also see the Appendix). Starting at a small amplitude $\mathscr{A}$, the goal is to obtain a whole family of steady-state solutions spanned by $\mathscr{A}$. To that end, the wave amplitude may be defined as $\mathscr{A}=\eta_{rms}=\psi_{rms}/c$, where η is the streamline displacement (see (2.10)) and *rms* denotes the root-mean-square value. Defined in this manner the amplitude contains a measure of both the vertical displacement and also the horizontal length of a given wave. By using the wave speed c_{wnl} from the weakly nonlinear solution, ψ may be scaled to have initial amplitude $\mathscr{A}_0$. Then subsequent states differ in amplitude by a specified $\delta\mathscr{A}$.

There are several advantages of using the amplitude as defined in this way ($\mathscr{A}=\eta_{rms}$) as the control variable spanning the family of solutions. First, it is a global, integrated measure of the wave amplitude. This allows the same definition to apply to any stable stratification without needing to impose a layered piecewise constant $N^2(Y)$ structure. Second, previous studies have often used wave speed c as a control variable (Fructus & Grue 2004), or alternatively the maximum vertical displacement of a given streamline (Brown & Christie 1998). While these control variables are easily compared with field observations, the approach is not ideal since (as shown below) these measures tend to constant values as the amplitude increases, thus rendering it increasingly difficult to distinguish between successive states in the computations. Another alternative would be to use the available potential energy of the wave (as defined later in § 3.3) as the control variable (following, e.g. Turkington *et al.* 1991; Lamb 2002). This is also an integrated measure and distinguishes well between states at large amplitude. However, there are problems with its use as the control variable in the numerical implementation used here. Firstly and least importantly, it distinguishes slightly more poorly than $\mathscr{A}$ between states at small amplitude. Secondly, the relationship between available potential energy, streamfunction and wave speed is not a simple one. So to determine wave speed at a given amplitude for a given streamfunction would require in general the solution of a complicated interrelated set of equations with, for example, a Newton–Raphson type method. This solution would be required at each iteration with no guarantee of good convergence properties particularly for larger amplitude waves and would considerably slow down the overall numerical solution. By contrast, when using η_{rms} as the control variable, finding the correct wave speed value is simple (see (2.25) below). The drawback is that η_{rms} is not a physically intuitive amplitude measure and direct comparison with observational data is not straightforward.

The initial guess for ψ and c is corrected by solving (2.11) for Y, followed by (2.21) for ζ at each point in the domain (using the previous guess for ψ in the right-hand side of (2.21)). Inverting $\nabla^2\psi = \zeta$ spectrally provides an updated value for ψ, and

$$c = \frac{\psi_{rms}}{\mathscr{A}}, \tag{2.25}$$

provides an updated value for c. This process is then repeated, by solving (2.11), (2.21) and (2.25) until ψ converges. In general, however, ψ does not converge, and relaxation is required. Therefore, the expression $\zeta = r\zeta_{new} + (1-r)\zeta_{old}$ is used, where ζ_{old} is the previous value for ζ and ζ_{new} is obtained from $\zeta_{new} = -N^2(Y)\psi_{old}/c^2$. The relaxation parameter $r < 1$ is allowed to vary in order to speed convergence. Here $r = 0.2(1 - n_i/n_{max})$, where n_i represents the current number of iterations in finding a particular steady state and n_{max} represents the maximum allowed number of iterations to find a state before the code is stopped ($n_{max} = 10\,000$). Typically, a few tens or hundreds of iterations are needed to find a steady state. However, finding the first steady state for which closed streamlines occur (when such a solution exists) can be more difficult, requiring more iterations. The relaxation scheme was also devised in order to overcome the convergence hurdle represented by finding the first state with closed streamlines. Progress beyond that point and convergence in general is more problematic without the relaxation as presented.

A solution ψ is accepted if the error, defined by the r.m.s. value of the change in ψ divided by ψ_{rms} is less than 1×10^{-7} (that is $(\psi - \psi_{old})_{rms}/\psi_{rms} < 1 \times 10^{-7}$, with the previous value of ψ_{old} found from $\nabla^{-2}\zeta_{old}$). The relative change of the absolute value of the difference $|\psi - \psi_{old}|/\psi_{max}$ is also monitored and found to be similarly small. Solutions obtained in this manner have been independently verified to be steady in a numerical code solving the unsteady system (2.4)–(2.6).

The interpolation of $N^2(Y)$ is performed on a grid 16 times finer than the y grid spacing used to represent ψ. Furthermore, the values of N^2 are found from cubic interpolation, using analytical values of N^2 and $\mathrm{d}N^2/\mathrm{d}Y$ on the fine grid. This ensures a highly accurate interpolation of N^2 in (2.21). Interpolation is employed in general, so that a measured profile (laboratory or observational) can be used as input. For the analytic profiles of N^2 described here the errors of the interpolation are of the order of machine precision.

Each of the numerical simulations is terminated when a wave amplitude is reached in which the wave fills half the domain horizontally, as defined by the spacing between the maximum and minimum of the vertical velocity field, v. Many of the solutions in § 3 exhibit the conjugate flow limit behaviour discussed by Lamb & Wan (1998), namely the waves exhibit a maximum vertical displacement at some amplitude and solutions beyond this amplitude simply broaden with a flat central region (the conjugate flow).

3. Results

Using the methodology outlined above, results are now presented for several different stratifications. Stratifications yielding ISWs of depression will be the focus, as ISWs of depression are more commonly observed in coastal oceans than ISWs of elevation (Ostrovsky & Stepanyants 1989). However, the methodology can equally well be applied to obtain solutions to stratifications that permit ISWs of elevation. In each of the calculations presented the computational grid used is 1024 points horizontally by 128 points vertically unless stated otherwise. The effect of changing

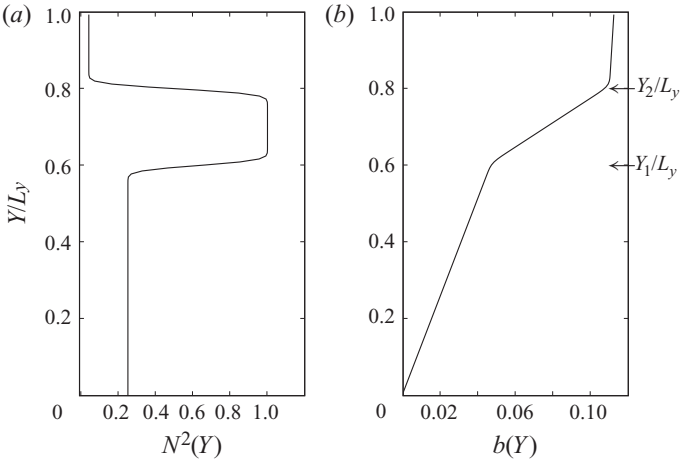

FIGURE 2. Plots of the profiles of N^2 left and b right for a layered stratified fluid with smoothing as defined in (3.1). The parameters used are $N_0^2 = 0.25$, $N_1^2 = 1$, $N_2^2 = 0.04$, $Y_1/L_y = 0.6$ and $Y_2/L_y = 0.8$ with a smoothing distance $\delta = 0.015625$, and a domain aspect ratio $L_y/2\pi = 0.05$.

the resolution is considered below and it is demonstrated that this choice of resolution is sufficient for the results presented.

3.1. *Layered stratification*

First solutions are presented for fluids consisting of either two or three linearly stratified layers. This allows comparison with the results of Fructus & Grue (2004), but moreover such flows are in themselves good models for many conditions found in the oceans. However, it should be noted that any smooth profile of $N^2(Y)$ can be used as input for the numerical scheme. A sharply stratified layered profile of $N^2(Y)$ can be generalized to allow for a degree of smoothing. This is accomplished by setting

$$N^2(Y) = \left(\frac{N_0^2 + N_2^2}{2}\right) + \left(\frac{N_1^2 - N_0^2}{2}\right)\mathrm{erf}\left(\frac{Y - Y_1}{\delta}\right) + \left(\frac{N_2^2 - N_1^2}{2}\right)\mathrm{erf}\left(\frac{Y - Y_2}{\delta}\right), \quad (3.1)$$

where erf denotes the error function, N_k^2 is the squared buoyancy frequencies in each of the three layers as in Fructus & Grue (2004) (with layers $k = 0, 1, 2$ being equivalent to layers 3, 2, 1 in Fructus & Grue (2004), respectively) and δ represents a distance over which the profile is smoothed using the above error function formulation. The layers are therefore numbered from the bottom upwards. This results in a profile which in general looks like that given in figure 2, where both buoyancy (obtained by integrating N^2) and buoyancy frequency squared are smooth. The lower layer has stratification given by N_0, the middle layer by N_1 and the top layer by N_2. The layer heights Y_1 and Y_2 mark the bottom and top of the middle layer, respectively. Smoothing can be suppressed by setting δ to a small number well below the finest grid size. However, convergence of the solution method then becomes problematic in some cases. In practice, a value of delta $\delta = 2\triangle y$ (or two y grid lengths) is taken. The effect of varying δ is discussed below.

The benefit of considering smooth profiles of $N^2(Y)$ is that the solutions obtained in this way are smoother vertically, and therefore exhibit negligible fringes in a spectral approach to inverting (2.21). This smoothness is also useful for accurately solving the weakly nonlinear problem (see the Appendix), here used as a first guess as described in § 2.2.

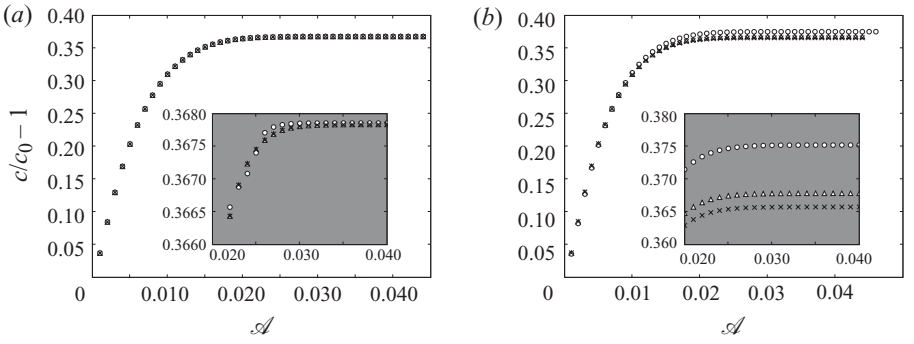

FIGURE 3. Plots of scaled wave speed $c/c_0 - 1$ versus amplitude, $\mathscr{A}$. (*a*) Effect of changing the resolution of the computation while keeping the smoothing distance $\delta/L_y = 2/128$ fixed. This smoothing length corresponds to two grid lengths in the standard resolution. (*b*) Effect of changing the resolution (as in plot (*a*)), where the smoothing is set always to be $\delta = 2\triangle y$, that is, two grid lengths of the given resolution. In each case, the symbols correspond to $\circ = (512 \times 64)$, $\triangle = (1024 \times 128)$ and $\times = (2048 \times 256)$ in resolution. The underlying set-up is three layers with $Y_1/L_y = 0.81$, $Y_2/L_y = 0.86$ and $N_0^2 = N_2^2 = 0$, $N_1^2 = 1$. In both plots, the grey regions are zoomed regions from the main plot to better see the differences between each of the curves.

Figure 3 shows the sensitivity of the wave speed to the resolution of the computation, in a typical case with $Y_1/L_y = 0.81$, $Y_2/L_y = 0.86$ and $N_0^2 = N_2^2 = 0$, $N_1^2 = 1$ (two neutral layers bounding a linearly stratified one). The wave speeds shown in figure 3 have been non-dimensionalized by dividing through by the linear long wave speed c_0 (the wave speed for linear waves with wavenumber zero – see the Appendix for more details of how this is obtained). In plot (*a*), the effect of keeping a fixed smoothing distance, in this case $\delta/L_y = 2/128$, while varying the resolution is considered. This smoothing length corresponds to two grid lengths in the standard resolution. This test measures how well the computations converge to the solution for a given smoothed profile. Results are shown for the resolutions $\circ = (512 \times 64)$, $\triangle = (1024 \times 128)$ and $\times = (2048 \times 256)$. It is found that there is very little difference between any of the resolutions and in particular that there is no benefit in moving from a resolution of (1024×128) to (2048×256) since there are no significant differences in the wave speeds when increasing resolution. In plot (*b*), the effect of changing the resolution while this time allowing the smoothing distance for the profile to change in step with the resolution is examined. The smoothing distance is set to be $\delta = 2\triangle y$, where $\triangle y$ is the grid length of a given resolution. This test illustrates how the results for smoothed profiles converge to those for a profile that has jumps in N^2 in the limit of infinite resolution. Plot (*b*) uses the same resolutions as in plot (*a*). As the resolution increases the curves get closer together, though now more slowly than in plot (*a*). Nevertheless, a convergent limit appears to exist. For practical reasons the resolution (1024×128) is used in subsequent calculations.

In figure 4, results for a three layer stratification with $N_0^2 = N_2^2 = 0$, $N_1^2 = 1$, and layer boundaries at the non-dimensional heights $Y_1/L_y = 0.81$ and $Y_2/L_y = 0.94$ are shown. A standard smoothing distance of two grid lengths is used in the profile of $N^2(Y)$. This stratification compares with Fructus & Grue (2004, figure 6). A wave with amplitude $\mathscr{A} = 0.011$ is shown, which gives $a/(L_y - Y_1) = 1.17$, where a is the maximum deflection of the streamline which coincides with the height Y_1 upstream. This wave therefore closely matches the wave shown in Fructus & Grue (2004) in

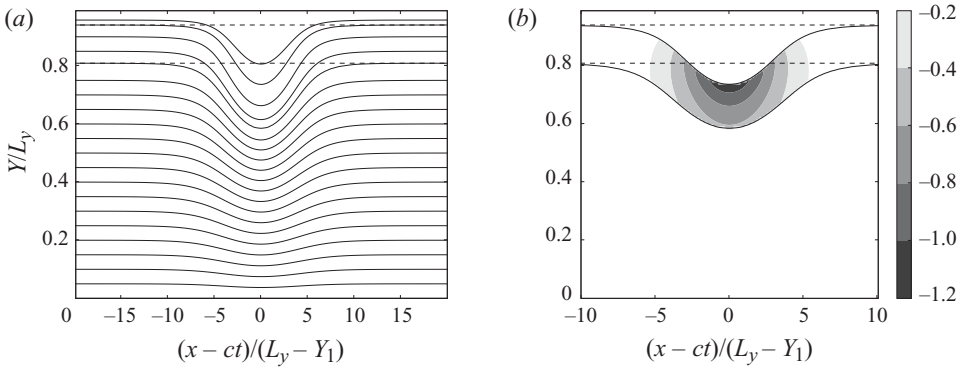

FIGURE 4. (*a*) The streamfunction, $\widetilde{\psi}$, and (*b*) scaled vorticity, $\zeta/(2\hat{N})$, for a three layer wave with layer height $Y_1/L_y = 0.81$ and $Y_2/L_y = 0.94$, and $N_0^2 = N_2^2 = 0$, $N_1^2 = 1$. The wave shown has amplitude $\mathscr{A} = 0.011$, and is matched in set-up and amplitude to that shown in Fructus & Grue (2004, figure 6). The bold lines are streamlines coinciding with the heights Y_1/L_y and Y_2/L_y at the domain edge, while dashed lines mark the layer heights Y_1/L_y and Y_2/L_y.

amplitude. The horizontal length scale is non-dimensionalized in the same manner as in Fructus & Grue (2004, figure 6), and the functions are plotted in the frame moving with the wave. In plot (*a*), contours of the streamfunction $\widetilde{\psi}$ in the moving frame are shown. The contour levels of streamfunction plotted are similar to those shown in Fructus & Grue (2004) and the layer heights $(Y_1/L_y, Y_2/L_y)$ are indicated by dashed lines. In plot (*b*), $\zeta/(2\hat{N})$ is shown for the same wave as in plot (*a*). The value of $\hat{N}$ is defined as in Fructus & Grue (2004), namely $\hat{N} = N_k\sqrt{1 - u/c}$, where N_k is the value of N for a given layer ($k = 0, 1, 2$) at the upstream domain edge. It should be noted that Fructus & Grue (2004) defined streamfunction in the opposite sense to the definition given in § 2 and so obtain positive vorticity values, while the values given here are negative. Both approaches are, however, consistent. The agreement between the plots shown in Fructus & Grue (2004, figures 4 and 6) is very good.

Finally for this stratification, plots of the Richardson number are presented. The Richardson number may be defined as

$$Ri = \frac{b_y}{\zeta^2}. \tag{3.2}$$

It represents the balance of stabilizing stratification to destabilizing shear forces. To obtain the Richardson number plots, a much finer resolution was used in the simulations, with a grid set at (2048×512) points and with a correspondingly small smoothing distance set at $2\triangle y$. This extra resolution was needed in order to resolve the area covered by $Ri < 0.25$ as this is a small region within the wave. In figure 5(*a*), a contour plot of the Richardson number is given, with the outer contour showing $Ri = 0.25$. It is well known that for $Ri > 0.25$ inviscid parallel shear flows must be stable to small disturbances and for $Ri < 0.25$ the flow is potentially unstable (Miles 1961). The wave shown is the largest calculated for this stratification and has amplitude $\mathscr{A} = 4.4 \times 10^{-2}$, which is equivalent to an amplitude $a/(L_y - Y_1) = 1.77$. Figure 5 (*a*) demonstrates that the minimum values of Ri occur near the top edge of the wave's pycnocline. This is in agreement with the computations presented in Fructus *et al.* (2009). The minimum Richardson number computed is $Ri = 0.062$. This is well below the 0.25 level which has proved difficult for other numerical methods to go beyond.

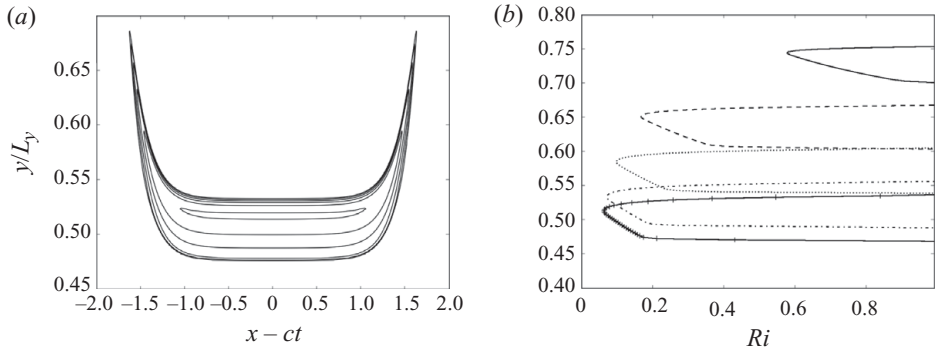

FIGURE 5. Plots of the Richardson number defined as in the main text. The stratification in both plots is such that $Y_1/L_y = 0.81$ and $Y_2/L_y = 0.94$, $N_0^2 = N_2^2 = 0$, $N_1^2 = 1$. (*a*) Contours of Ri for a wave with amplitude $\mathscr{A} = 4.4 \times 10^{-2}$; the outer contour is for $Ri = 0.25$, and six contours are presented, evenly spaced in Ri down to the contour $Ri = 0.065$. The outer two (in some regions three) contours are almost indistinguishable since Ri changes sharply at the edge of the wave. (*b*) Ri along cross-sections through the middle ($x = 0$) of waves with amplitudes $\mathscr{A} = 5 \times 10^{-3}$ (—), 1×10^{-2} (——), 1.5×10^{-2} (· · ·), 2.2×10^{-2} (— · —), and 4.4×10^{-2} (—+—).

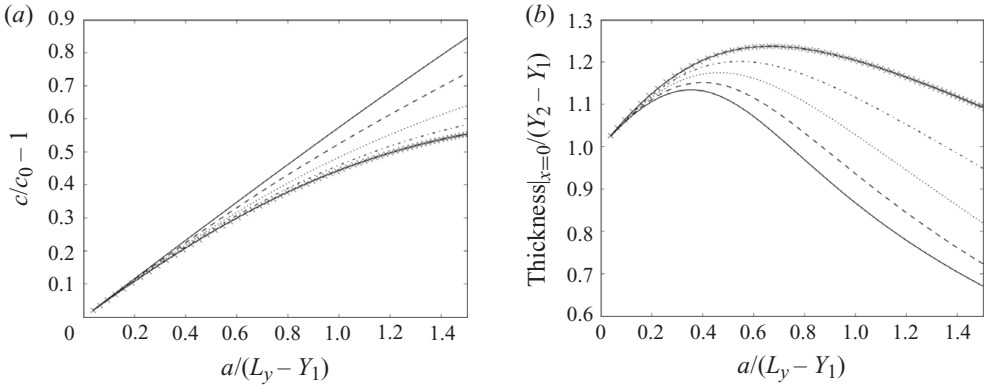

FIGURE 6. (*a*) Non-dimensionalized wave speed versus amplitude and (*b*) pycnocline thickness at the midpoint of the wave versus amplitude. In both plots, the amplitude measure is that used in Fructus & Grue (2004), to compare to their figure 9*c*. The stratification is such that $Y_1/L_y = 0.81$ and $Y_2/L_y = 0.94$, $N_0^2 = 0$, $N_1^2 = 1$. The different curves represent different values of N_2: $N_2 =$ 0 (-×-), 0.5 (— · —), 0.7 (· · ·), 0.87 (– –), and 1.0 (—).

In figure 5(*b*), cross-sections of Richardson number through the centre of the wave are given for waves of different amplitudes as indicated. These curves demonstrate that as amplitude increases the minimum Richardson number gets smaller, and the low-Richardson number-region moves down in the domain following the region, where streamlines reach their maximum excursion.

A further comparison with the results of Fructus & Grue (2004) is made in figure 6, showing results for a stratification with layer boundaries at the non-dimensional heights $Y_1/L_y = 0.81$ and $Y_2/L_y = 0.94$. Here, $N_0 = 0$ and $N_1 = 1$ are fixed, while N_2 takes values $N_2 = 0$, 0.5, 0.7, 0.87 and 1.0 as indicated. The smoothing distance used in the profile of $N^2(Y)$ was set to be one grid length as this more closely matches the stratification in Fructus & Grue (2004) (this sharper transition was found to be important in determining pycnocline thickness, shown in figure 6*b*). In order to

reproduce the curves given in Fructus & Grue (2004), the extension of $N^2(Y)$ for closed streamlines outlined in (2.22) has been used. The current figure can be compared with Fructus & Grue (2004, figure 9*c*). Figure 6(*a*) shows the non-dimensionalized wave speed against the measure of amplitude used by Fructus & Grue (2004), namely $a/(L_y - Y_1)$, where a is once again the maximum deflection of the streamline which coincides with the height Y_1 upstream. The wave speed in plot (*a*) has been non-dimensionalized by dividing through by the linear long wave speed c_0. In plot (*b*), the thickness of the pycnocline (the region bounded by the streamlines traced from heights Y_1 and Y_2 upstream) at the wave midpoint is shown. Once again the plot is against the amplitude measure preferred by Fructus & Grue (2004) and is given in order to compare to their results. Both plots show good agreement with Fructus & Grue (2004, figure 9*c*). Very small differences are seen in the curves and can be attributed to the smoothing length used in the method presented here. Also note that the plots shown are continued for larger amplitudes than those given by Fructus & Grue (2004).

Next the effect of using the different continuations for $N^2(Y)$ relevant to dealing with closed streamlines as discussed in § 2.1 are examined. A two layered stratification with $Y_1/L_y = 0.81$, $Y_2/L_y = 0.94$, $N_0^2 = 0$ and $N_2^2 = N_1^2 = 1$ is considered. No change in stratification occurs at Y_2, but it is set so that the streamline plots produced may be compared to Fructus & Grue (2004, figure 15). The smoothing distance δ was set to one grid length. The smoothing distance to the extension outside the domain W was set to $10^{-9}L_y$. In § 2.1, three different options for the steady-state solution were considered. The first option assumes non-constant vorticity and buoyancy across the closed streamline region, and arises from continuing $N^2(Y)$ at a constant value, and using (2.21) to solve within the region. The other two options both assume constant buoyancy across the closed streamline region, the first of these has zero vorticity across this region and the second assumes constant vorticity of a value determined by conditions at the upstream domain edge. First the new solution with a zero vorticity core will be compared to the solution with non-constant buoyancy within the core. Then solutions with non-zero vorticity cores will be discussed.

In figure 7, the results of the two different continuations for $N^2(Y)$ detailed in § 2.1 are shown. In particular, plot (*a*) shows the streamlines resulting from using (2.23) while plot (*b*) shows those resulting from using (2.22). Plot (*b*) corresponds to the larger amplitude wave plotted by Fructus & Grue (2004, figure 15). Both plots (*a*) and (*b*) are generated using equal intervals for the levels of the streamfunction. The lack of closed streamlines in plot (*a*) is, therefore, a real feature of the flow. Effectively the core region of the flow is stagnant in the moving frame with a constant density and zero vorticity.

The differences between the two approaches are further outlined in figure 8. In figure 8(*a*), the non-dimensionalized wave speed is plotted as a function of wave amplitude $\mathscr{A}$ and in plot (*b*) the maximum value of the non-dimensionalized horizontal velocity u/c is plotted, again as a function of amplitude. In both plots, the approach outlined in (2.23) is shown with a solid line, while that outlined in (2.22) is shown with a dashed line. The background stratification for the waves computed in figure 8 is the same as in figure 7. Plot (*a*) shows that the effect of the new approach is that the wave speed c is less than in the previous model when closed streamlines (or now more accurately stagnant patches) start to appear within the flow. Plot (*b*) also demonstrates that while the dimensionless horizontal velocity keeps increasing for the approach previously used (2.22), the new approach shows that u/c is sharply bounded by unity, so that the horizontal velocity never exceeds the wave speed. Note

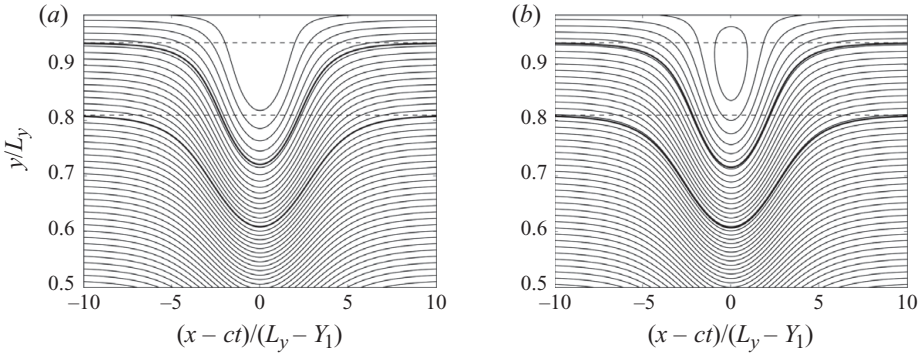

FIGURE 7. Plots of the streamlines for a wave with amplitude $\mathscr{A} = 0.009$, with equal intervals of 2×10^{-4} chosen for the levels of the streamfunction. Only the top half of the domain is shown. The underlying stratification for the computations is $Y_1/L_y = 0.81$, $Y_2/L_y = 0.94$ and $N_0^2 = 0$, with $N_2^2 = N_1^2 = 1$, giving a two layered structure. Both layer heights are plotted although the upper layer height does not correspond to a change in stratification. The layer heights Y_1/L_y and Y_2/L_y are plotted with dashed lines. (*a*) Calculation performed with the procedure outlined by (2.23), while (*b*) was obtained by the use of (2.22). (*b*) Corresponds to the larger amplitude case plotted by Fructus & Grue (2004, figure 15).

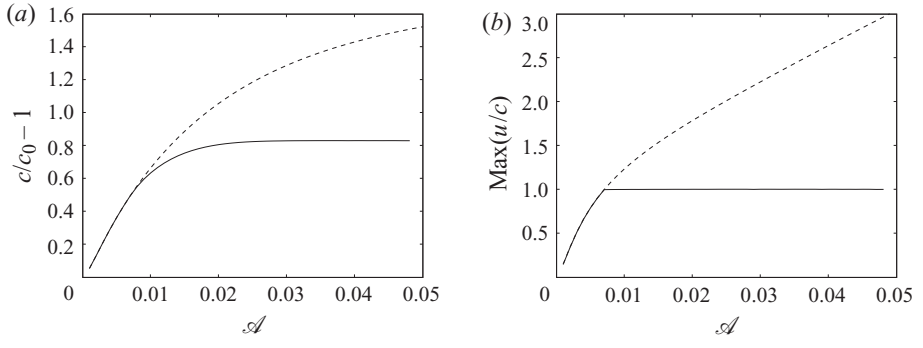

FIGURE 8. (*a*) Non-dimensional wave speed versus the amplitude of the wave, $\mathscr{A}$. (*b*) Maximum dimensionless horizontal velocity u/c versus $\mathscr{A}$. In both plots, the approach outlined in (2.23) having a uniform density core is shown by a solid line, while that outlined in (2.22) is shown by a dashed line. The background stratification for these waves is $Y_1/L_y = 0.81$, $Y_2/L_y = 0.94$ and $N_0^2 = 0$, with $N_2^2 = N_1^2 = 1$, as in figure 7 above.

that if $u/c > 1$ the flow will be convectively unstable and therefore the steady state predicted from (2.21) is not in fact realisable. Both Brown & Christie (1998) and Fructus & Grue (2004) acknowledge this contradiction in their work.

Figure 9 shows the streamlines associated with a wave having a constant density and constant non-zero vorticity core. This wave has the same amplitude as those in figure 7, and is found using the methodology discussed in § 2.1. The constant vorticity in the core is found using (2.24). The extra closed streamlines seen in the core demonstrate that for this wave the re-circulating flow is much stronger than in the waves seen in figure 7.

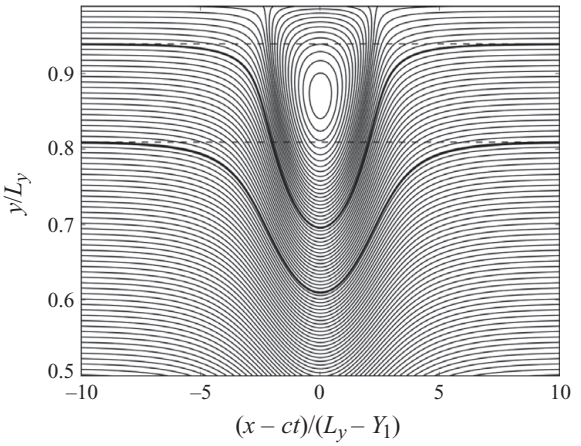

FIGURE 9. Plots of the streamlines for a wave with amplitude $\mathscr{A} = 0.009$, with equal intervals of 2×10^{-4} chosen for the levels of the streamfunction. Only the top half of the domain is shown. The underlying stratification and line styles are as for figure 7. This wave has a constant density, but non-zero constant vorticity core as discussed in § 2.1.

3.2. *Flow evolution*

In figures 10–12 (and in the supplementary movies available at journals.cambridge.org/flm), simulations of the time evolution of the states plotted in figures 7(*a*), 7(*b*) and 9 are presented, respectively. The waves shown in each of these figures propagate from left to right. The time evolution is computed by solving the vorticity formulation of (2.4)–(2.6), including a weak ∇^6 hyperdiffusion on vorticity (with diffusion coefficient 512^{-6}) in order to stabilize the solution. The unsteady numerical simulations were carried out using CLAM, an accurate numerical method using contour advection (Dritschel & Ambaum 1997) to evolve the buoyancy field conservatively. Details of the numerical method used in these figures may be found in Dritschel & Fontane (2010). Further analysis of the unsteady behaviour of such ISWs is the subject of current work. Figures 10–12 (movies 1–3, respectively) contain sequences of plots of the vorticity distribution within the wave. The consequences of the three different approaches outlined in § 2.1 for dealing with flows in which closed streamlines may occur are apparent in the first frame. The new approach (figure 10) has a region of zero vorticity in the top part of the upper layer, where the flow is stagnant. The previous approach (figure 11) has non-zero vorticity throughout the closed streamline region. The approach leading to a rotating core of constant buoyancy and constant non-zero vorticity (figure 12) has a larger core region with a comparatively large value of vorticity throughout. Figures 10–12 show weak fringing of positive vorticity around the edges of the pycnocline where there are sharp gradients of vorticity and buoyancy. The fringing is caused by these sharp gradients along with the diffusion of vorticity required to stabilize the numerical scheme. If a smoother underlying profile of the background buoyancy is used the appearance of these fringes can be reduced. Nevertheless it is evident that the new approach with zero vorticity in the closed streamline region (figure 10) is substantially more stable than the approach used previously by Brown & Christie (1998) and Fructus & Grue (2004) (figure 11), and the approach with a constant vorticity rotating core (figure 12). In particular, the case with non-constant buoyancy throughout the closed streamline region (figure 11), which was noticed previously to be statically unstable is indeed subject to an instability

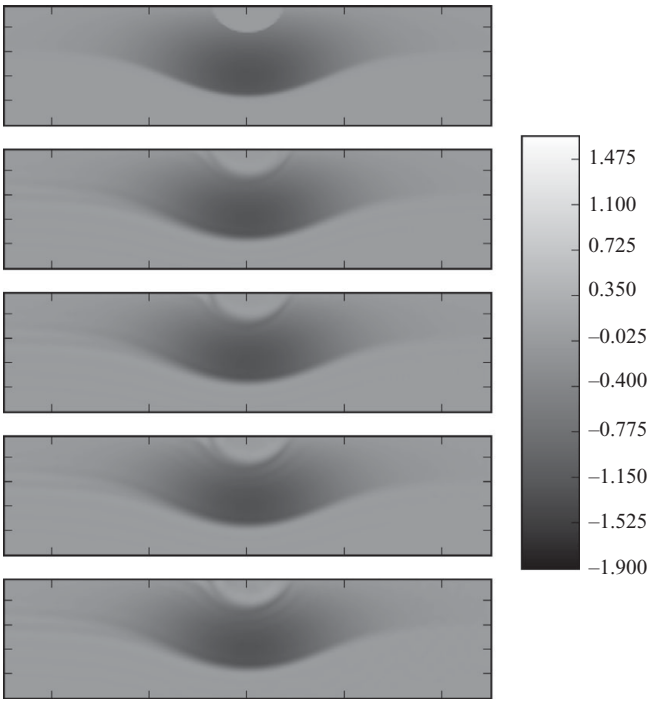

FIGURE 10. Sequence showing the nonlinear evolution of the vorticity field, ζ, for the steady state pictured in figure 7(a). Each successive plot is at a later time (times $t =$ 0, 25, 50, 75 and 100, time increasing downwards), with the total time of integration being approximately equivalent to the time the wave would take to move one and a half times through the full computational domain. The axes labels are omitted for clarity, however, the region of the domain shown is $(x, y/L_y) \in [-0.5, 0.5] \times [0.5, 1.0]$. See also supplementary movie 1.

and mixes the zone where closed streamlines were predicted. In the new approach (figure 10), the stagnant region remains stable and stagnant despite the appearance of fringes of positive vorticity arising from the sharp gradients in buoyancy around the edge of the closed streamline region. The rotating core solution can also be seen to be unsteady (figure 12). A disturbance to the flow starts at the top left of the wave and is subsequently advected around the central vortex core. This modifies the structure of the original wave and causes it to slow slightly.

To better understand this flow adjustment, a schematic diagram of the streamline pattern for any wave with a rotating core of fluid is illustrated in figure 13. Stable and unstable streamline configurations appear as marked in figure 13. At the front of the wave, fluid particles accelerate away from the wall. This is a stable process in the sense that two particles initially near each other will remain so. At the back of the wave where streamlines impinge on the wall particles decelerate towards the wall which is an unstable process. Here particles may be swept either to the left or to the right, depending sensitively on their exact position. This is analogous to the instability occurring in two-dimensional dipoles (Dritschel 1995). The similarity can be seen by simply considering the rigid boundary of this problem as the mid plane of the problem in Dritschel (1995) and reflecting the streamlines about it.

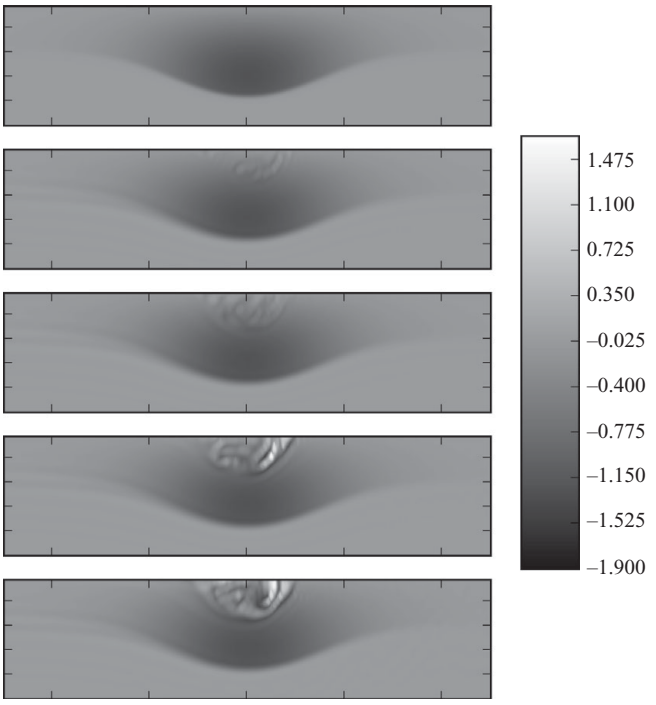

FIGURE 11. As in figure 10, but starting from the steady state shown in figure 7(*b*). See also supplementary movie 2.

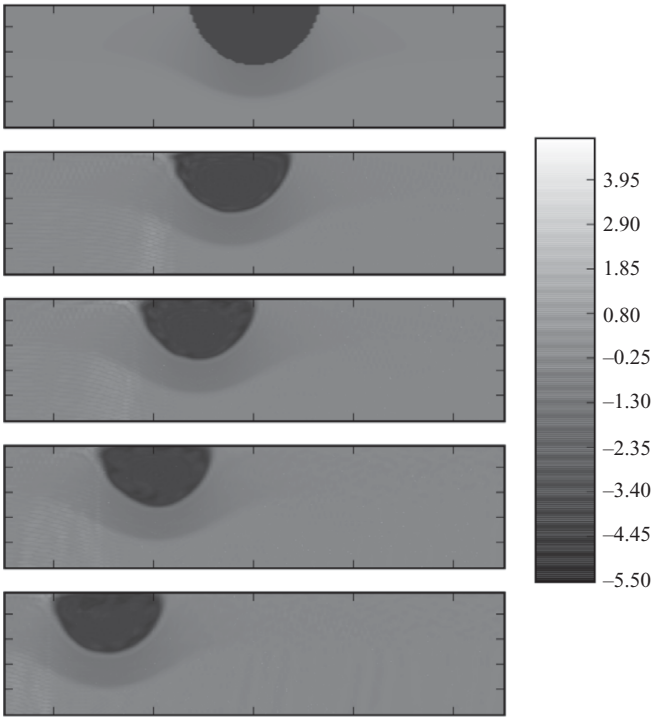

FIGURE 12. As in figure 10, but starting from the steady state shown in figure 9. See also supplementary movie 3.

Layer heights Y_1/L_y, Y_2/L_y	Layerwise N values	Symbol used in plots
0.7, 0.75	0, 1, 0	(—)
0.75, 0.8	0, 1, 0	(– –)
0.8, 0.85	0, 1, 0	(- -)
0.85, 0.9	0, 1, 0	(· · ·)
0.9, 0.95	0, 1, 0	(—·)

TABLE 1. Values of the parameters used in the first set of steady-state solutions. These runs simply vary the height of the pycnocline up and down.

Layer heights Y_1/L_y, Y_2/L_y	Layerwise N values	Symbol used in plots
0.81, 0.86	0, 1, 0.25	(—)
0.81, 0.86	0, 1, 0.5	(– –)
0.81, 0.86	0, 1, 0.75	(- -)
0.81, 0.86	0, 1, 1	(· · ·)
0.81, 0.86	0, 1, 1.25	(—·)

TABLE 2. Values of the parameters used in the second set of steady-state solutions. These runs keep the pycnocline height fixed and vary the value of N in the top layer.

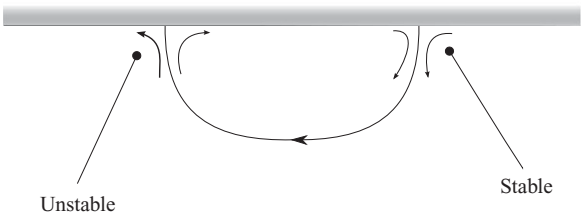

FIGURE 13. Schematic diagram showing the structure of streamlines for a steady-state solution with a rotating core of fluid in a region of closed streamlines. The stable and unstable streamline configurations are marked on the diagram. This diagram can also be compared with the streamlines shown in figure 9.

3.3. *Wave properties*

Two sets of steady-state wave solutions are compared next. This is done in order to elicit the effect of simple changes to one of the parameters in a layered background stratification. To see the result of such changes various characteristic quantities of the flow (such as wave speed or energy) are plotted as a function of wave amplitude. The results presented are for a three layer background stratification. The parameter values are summarized in tables 1 and 2. In the first set of solutions (table 1), the level of the pycnocline is varied from just below three quarters of the domain height to near the top of the domain. The pycnocline thickness remains unvaried at $0.05L_y$. That is, the distance $Y_2 - Y_1$ remains fixed at $0.05L_y$, while the heights Y_1 and Y_2 are allowed to vary from just below three quarters of the domain height to near the top of the domain. The stratification in this set has the buoyancy constant ($N^2 = 0$) in the upper and lower layers and $N^2 = 1$ within the pycnocline. For the second set of solutions (table 2), the pycnocline is kept at a fixed height and location. The value of N^2 is fixed at 0 in the lower layer, at 1 within the pycnocline and systematically increased in the top layer. In all of the computations, the smoothing length for the

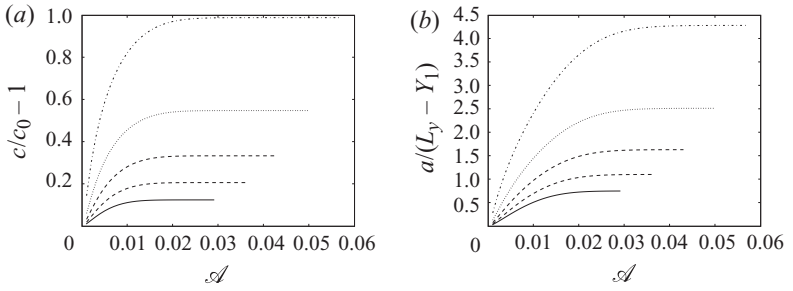

FIGURE 14. (*a*) Non-dimensionalized wave speed versus the amplitude of the wave, $\mathscr{A}$. (*b*) A typical measure of amplitude used in many previous studies ($a/(L_y - Y_1)$, where a is the maximum deflection of the streamline which coincides with the height Y_1 upstream) plotted against the current amplitude measure $\mathscr{A}$. The plot is for parameter values and line styles as given in table 1.

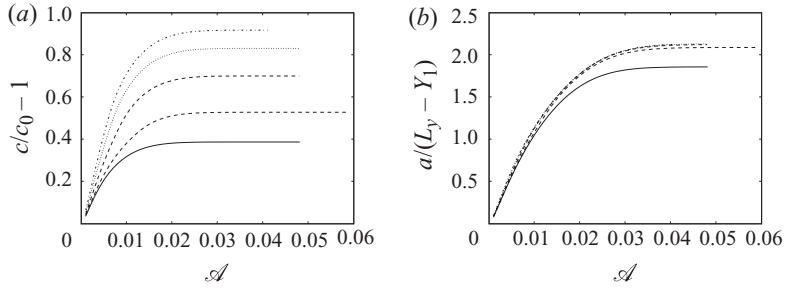

FIGURE 15. (*a*) Non-dimensionalized wave speed against the amplitude of the wave, $\mathscr{A}$. (*b*) A typical measure of amplitude used in many previous studies ($a/(L_y - Y_1)$, where a is the maximum deflection of the streamline which coincides with the height Y_1 upstream) plotted against the current amplitude measure $\mathscr{A}$. The plot is for parameter values and line styles as given in table 2.

profile of $N^2(Y)$ was set to two grid lengths: $\delta = 2L_y/128$. The smoothing distance W to the continuation of $N^2(Y)$ outside the domain was taken to be $10^{-9}L_y$.

Various properties of these solutions are plotted in figures 14–19. Figure 14 shows (i) the non-dimensional wave speed against $\mathscr{A}$ and (ii) the measure of amplitude used by various other authors (namely $a/(L_y - Y_1)$, where a is the maximum deflection of the streamline with height Y_1 upstream) as a function of wave amplitude $\mathscr{A}$ for the cases in table 1. Figure 15 shows the same quantities for the cases in table 2. In both sets of cases, the quantities considered all tend to constant values at large wave amplitudes. Figure 14 shows that the effect of raising the pycnocline height is (i) to increase the wave speed and (ii) to increase the vertical excursion of the streamlines. Similarly figure 15 shows that the effect of strengthening the stratification in the top layer is to increase the wave speed while no monotonic change is seen in the vertical excursion of the streamlines. In both cases, the streamline deflection shown in figures 14(*b*) and 15(*b*) tends to a constant value at large amplitude which is suggestive that the conjugate flow limit has been reached.

Following Lamb & Nguyen (2009), the energy associated with the wave can be defined as the sum of the kinetic energy and the available potential energy. The pseudoenergy defined in this way reflects that not all of the potential energy in the system is available to be converted into kinetic energy. The expression for

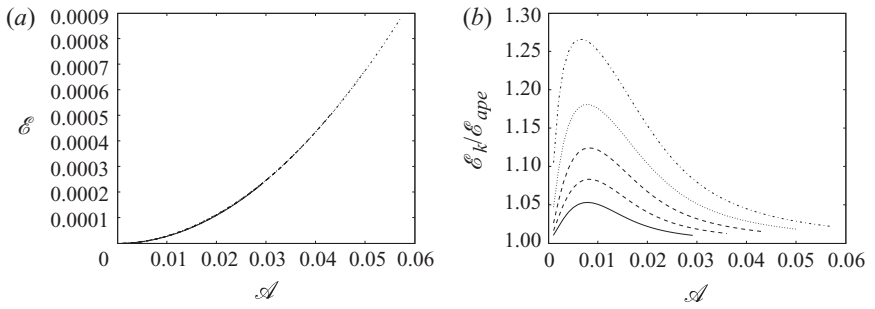

FIGURE 16. (*a*) The total energy $\mathscr{E}$ (kinetic plus available potential energy, see (3.3)) contained in the wave plotted as a function of wave amplitude, $\mathscr{A}$. (*b*) The ratio of kinetic energy to available potential energy $\mathscr{E}_k/\mathscr{E}_{ape}$ versus $\mathscr{A}$. The parameters and line styles are given in table 1.

pseudoenergy is

$$\mathscr{E} = \iint_{\mathscr{D}} \left(\frac{1}{2}(u^2 + v^2) + E_{ape} \right) \mathrm{d}x\, \mathrm{d}y, \tag{3.3}$$

where E_{ape} is the available potential energy density and $\mathscr{D}$ represents the domain over which the solution is defined. Similarly integrals of the kinetic and available potential energy may be defined, respectively, by

$$\mathscr{E}_k = \iint_{\mathscr{D}} \frac{1}{2}(u^2 + v^2)\, \mathrm{d}x\, \mathrm{d}y \quad \text{and} \quad \mathscr{E}_{ape} = \iint_{\mathscr{D}} E_{ape}\, \mathrm{d}x\, \mathrm{d}y. \tag{3.4}$$

Using the method for obtaining available potential energy outlined in Lamb (2008) gives

$$E_{ape}(x, y) = \int_y^{Y(x,y)} (b(x, y) - \bar{b}(s))\, \mathrm{d}s. \tag{3.5}$$

Figure 16(*a*) shows the total energy associated with the wave as a function of wave amplitude, using the definitions in (3.3) and (3.5), while figure 16(*b*) shows the ratio of kinetic energy to available potential energy using (3.4) and (3.5). Both plots (*a*) and (*b*) in figure 16 are for the cases in table 1. Figure 17 shows the corresponding results for the cases in table 2. From figure 16, it can be seen that simply moving the pycnocline up has little effect on the total energy in the wave; it does, however, change the balance of kinetic and available potential energy. As the pycnocline moves up the wave contains more kinetic energy, which was previously found by Lamb & Nguyen (2009). In figure 17, it can be seen that as the stratification in the top layer strengthens the energy content of the wave increases, particularly the kinetic energy content. In all cases the ratio of kinetic energy to available potential energy is found to be greater than unity as found previously by Turkington *et al.* (1991) and Lamb & Nguyen (2009).

Figure 18(*a*) shows the circulation Γ associated with a given wave, defined as

$$\Gamma = \iint_{\mathscr{D}} \zeta\, \mathrm{d}x\, \mathrm{d}y, \tag{3.6}$$

versus $\mathscr{A}$, while figure 18(*b*) shows the integrated buoyancy anomaly, $\mathscr{Q}$, defined as

$$\mathscr{Q} = \iint_{\mathscr{D}} (b(x, y) - \bar{b}(y))\, \mathrm{d}x\, \mathrm{d}y, \tag{3.7}$$

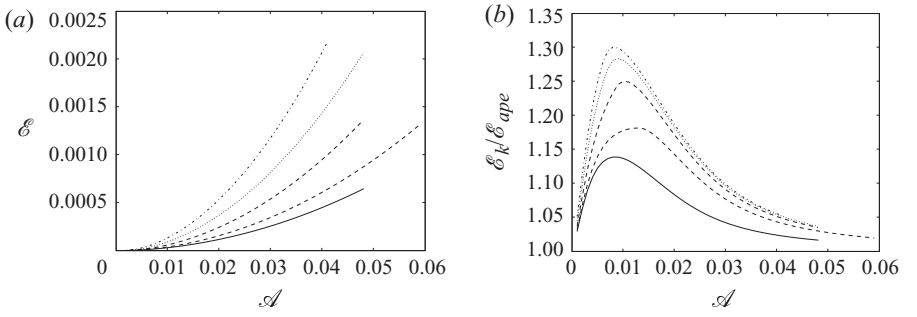

FIGURE 17. (*a*) The total energy $\mathscr{E}$ and (*b*) the ratio of kinetic energy to available potential energy $\mathscr{E}_k/\mathscr{E}_{ape}$ versus $\mathscr{A}$ for the set of cases given in table 2.

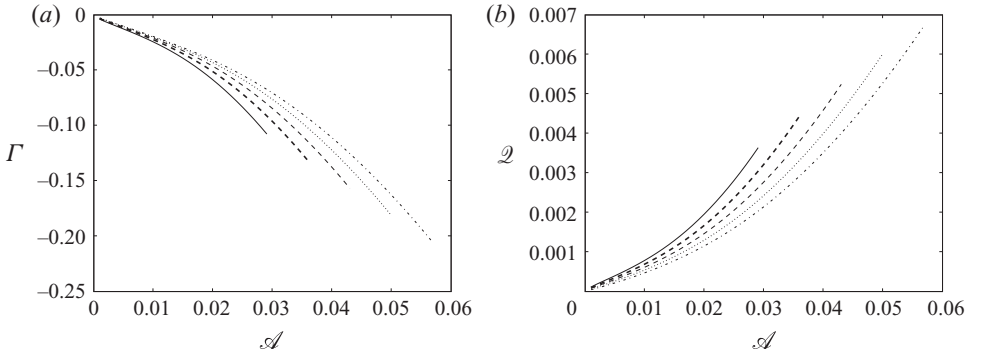

FIGURE 18. (*a*) Circulation Γ (see (3.6)) and (*b*) buoyancy anomaly $\mathscr{Q}$ (see (3.7)) versus $\mathscr{A}$. In both plots, the parameters and the line styles used are given in table 1.

versus $\mathscr{A}$. Both quantities are shown for the cases in table 1. The circulation, like the energy, is an invariant of the flow. It becomes increasingly large and negative as the wave amplitude increases. The buoyancy anomaly is proportional to the mass contained within the wave and this increases in a similar manner to the total energy (see figure 16) as the wave amplitude increases.

Using the integrated quantities $\mathscr{E}$, $\mathscr{Q}$ and Γ, with the wave speed c it is possible to construct length scales characterizing the waves. These length scales may be useful since they may be evaluated for arbitrary stratification. Also as they are integrated quantities they are insensitive to the detailed structure of the wave. Therefore they may be practically useful for observations of waves having associated measurement error. Moreover they are constructed from integral invariants of the wave, which is commonly done in various fluid dynamical problems to obtain characteristic length and time scales for a given flow. Four length scales can readily be constructed, namely:

$$L_1 = \frac{\sqrt{2\mathscr{E}}}{c}, \quad L_2 = \frac{\mathscr{Q}}{c^2}, \quad L_3 = \frac{\Gamma^2}{\mathscr{Q}}, \quad L_4 = \frac{\mathscr{E}}{\mathscr{Q}}. \tag{3.8}$$

Figure 19(*a–d*) shows $L_1, \ldots, L_4$, respectively, for the cases in table 1. It is clear that L_4 represents some vertical extent of the wave since L_4 tends to a constant value at large amplitude and is much smaller in magnitude than the other length scales. The scale L_1 depends only weakly on changes in stratification and is linear, implying it carries much the same information as the amplitude $\mathscr{A}$. The last two scales L_2 and

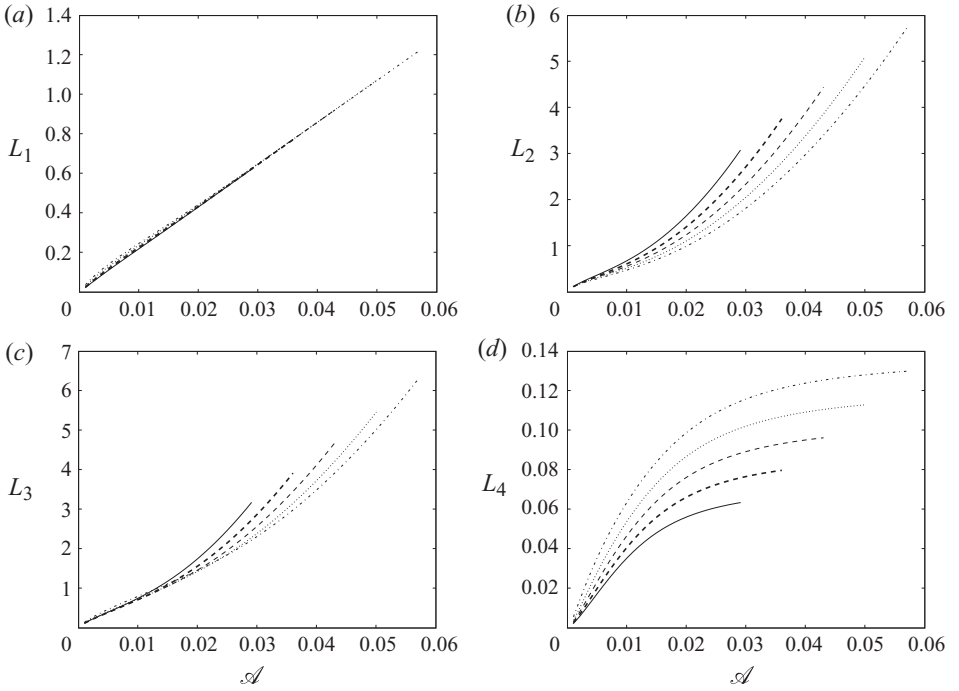

FIGURE 19. (a–d) Length scales L_1–L_4 as defined in the text. Parameter values and the line styles used for the plots are taken from table 1.

L_3 increase as the horizontal scale of the wave does. Thus they provide a measure of the length of the wave.

3.4. *A smooth ocean-like stratification*

An alternative profile for $N^2(Y)$ is now considered, of the form

$$N^2(Y) = N_0^2 \exp(\alpha_0 Y/L_y)\operatorname{erfc}\left(\beta_0\left(\frac{Y}{L_y} - Y_0\right)\right), \tag{3.9}$$

where erfc denotes the complementary error function and N_0^2 is chosen so that the maximum value of N^2 is unity. The parameters α_0, β_0 and Y_0 are chosen so that the profile resembles the measured ocean stratification in Stanton & Ostrovsky (1998) without any direct reference to layer heights. The profile is shown in figure 20 and consists of a small well-mixed layer of fluid at the surface, overlying a smooth transition into a sharply stratified region, below which the strength of the stratification decays towards the bottom of the domain.

Figure 21 illustrates various fields associated with a large-amplitude ISW in this stratification. The wave considered has amplitude $\mathscr{A} = 0.0395$ and the parameters used to set-up the background stratification using (3.9) are $\alpha_0 = 3$, $\beta_0 = 30$ and $Y_0 = 0.9$. In plot (a), the vorticity ζ is shown and in plot (b) the squared buoyancy frequency N^2 is shown. Both quantities exhibit the broad flat-topped nature of the wave, which is typical of large-amplitude ISWs limited by a conjugate flow (Lamb & Wan 1998). In plots (c) and (d), the u and v components of the velocity field are presented, respectively. In (c), the shear layer at the centre of the wave is evident. Finally, in (d)

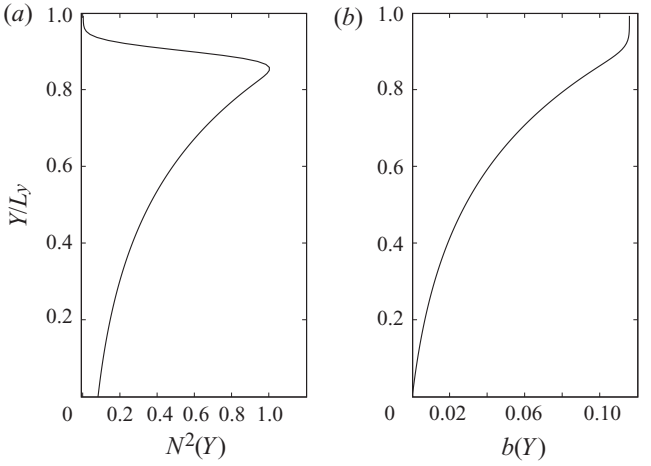

FIGURE 20. Plots of both the profiles of $N^2(Y)$ and $b(Y)$ for a fluid stratified according to (3.9). The parameters used for the plot have values $\alpha_0 = 3$, $\beta_0 = 30$ and $Y_0 = 0.9$, and the domain has aspect ratio 0.05.

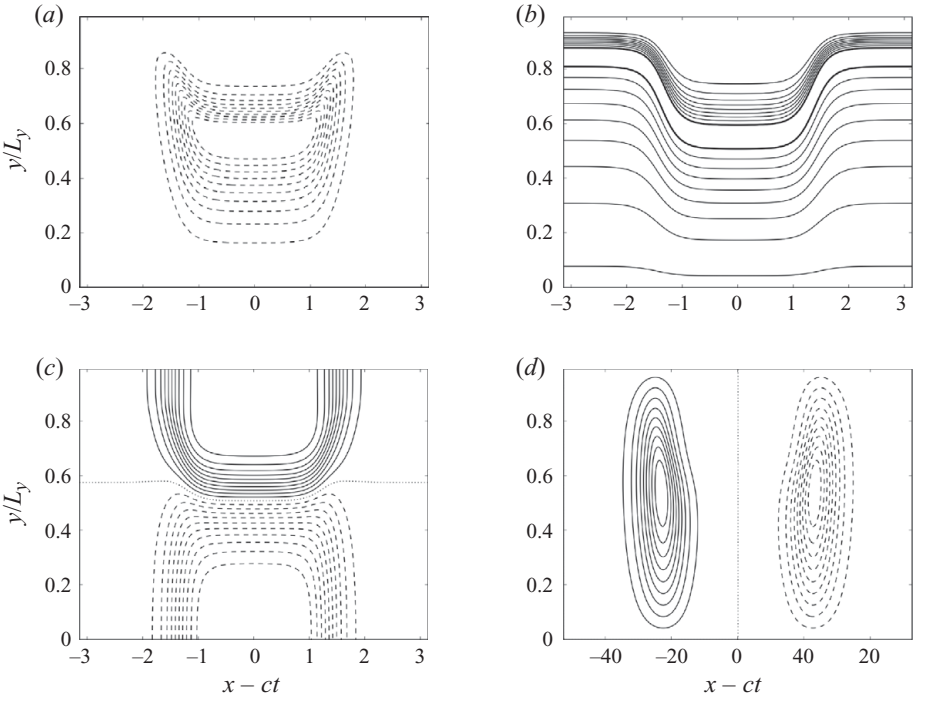

FIGURE 21. (*a*) ζ, (*b*) N^2, (*c*) $u - c$ and (*d*) v for a wave with amplitude $\mathscr{A} = 0.0395$, in a background stratification given by (3.9), with $\alpha_0 = 3$, $\beta_0 = 30$ and $Y_0 = 0.9$. The contours are solid for positive values, dashed for negative and dotted for the zero contour, where it is shown. The contours shown are (*a*) $-0.1 \to -1.0$ with contour interval 0.1, (*b*) $0.1 \to 0.9$ with contour interval 0.1 and the 0.9 contour picked out in bold, (*c*) and (*d*) contours are evenly spaced working from the zero contour, with contour intervals 0.005 and 0.001, respectively.

the previous use made of the distance between the global maximum and minimum of the v component of velocity to define a length scale for the wave can be seen to be justified.

4. Summary

A new method of finding the steady-state form of ISWs in a stratified fluid has been presented. This method is significantly simpler than previous methods (Turkington *et al.* 1991; Fructus & Grue 2004), as it only involves the inversion of Laplace's operator in spectral space rather than solving a variational problem or complicated integral equations. The cost of this simplicity is that the stratification needs to be smooth, that is, $N^2(Y)$ must be a smooth function. It has been demonstrated, however, that with a suitable choice of smoothing it is possible to closely approximate a sharply layered stratification. As part of this new method, a new amplitude measure has been introduced. This measure appears to be more robust than previous measures of wave amplitude in that it does not explicitly depend on a given background stratification and it continues to increase for large-amplitude waves when other commonly used amplitude measures tend to constant values. In turn this allows a clearer discrimination between different large-amplitude waves. The new method is not limited by small Richardson numbers. Waves with values of the Richardson number as low as 0.062 were computed. In addition, a new approach for dealing with flows containing closed streamlines was presented. In particular, the new approach allows for a region of constant buoyancy or equivalently density, and zero vorticity. The region moves as a trapped, nearly stagnant core translating at the wave speed, rather than as a recirculating core of fluid having a large region of statically unstable fluid. Waves having constant buoyancy and non-zero vorticity cores were also considered and unsteady simulations of three different cases were presented. The unsteady numerical simulations exhibit striking differences between a constant density core and a non-constant density core: the latter is considerably less steady and breaks down violently. Similarly, waves with a non-zero constant vorticity core were observed to destabilize near the rear stagnation point of the wave. The instability is less violent and appears to lead to an adjusted quasi-steady wave. A more thorough investigation of the nonlinear evolution of ISWs will be the focus of further experimental and numerical work.

The authors are grateful for support from the UK Engineering and Physical Sciences Research Council under its Mathematical Sciences Programme (grant number EP/F030622/1). The helpful comments of four anonymous referees are also gratefully acknowledged.

Supplementary movies available at journals.cambridge.org/flm.

Appendix

The initial guesses for the wave speed and the streamfunction provided to the fully nonlinear wave computations are given by weakly nonlinear KdV theory. The KdV theory comes from an appropriate long wave, small amplitude scaling of the model equations, and the well-known sech^2 form of solitary wave is obtained as the relevant solution. Following the solution given in Benney (1966) this gives

$$\psi(x, y, t) = -a(x, t)c_{wnl}\phi(y), \tag{A 1}$$

where $a(x, t)$ is a solution to the KdV equation ($a_t + c_0 a_x + \alpha_0 a a_x + \beta a_{xxx} = 0$), c_{wnl} is the phase speed of the wave and $\phi(y)$ is the solution to the linear eigenproblem for

the wave with zero horizontal wavenumber

$$\frac{\mathrm{d}^2\phi}{\mathrm{d}y^2} + \frac{N^2(y)}{c_0^2}\phi = 0, \tag{A 2}$$

subject to $\phi(0) = \phi(L_y) = 0$. Here c_0 is the linear long wave speed associated with this mode (c_0^{-2} is the eigenvalue). The simple solitary wave solution to the KdV equation is

$$a(x,t) = \widehat{a}_0 \mathrm{sech}^2\left(\frac{x - c_{wnl}t}{\lambda}\right), \tag{A 3}$$

where $\widehat{a}_0$ is a given amplitude, $c_{wnl} = c_0 + \widehat{a}_0\alpha_0/3$ and $\lambda^2 = 12\beta/\widehat{a}_0\alpha_0$. The constants α_0 and β appearing in the coefficients of the KdV equation above are given by

$$\alpha_0 = \frac{3c_0\displaystyle\int_0^{L_y}\phi_y^3\,\mathrm{d}y}{2\displaystyle\int_0^{L_y}\phi_y^2\,\mathrm{d}y}, \tag{A 4}$$

$$\beta = \frac{c_0\displaystyle\int_0^{L_y}\phi^2\,\mathrm{d}y}{2\displaystyle\int_0^{L_y}\phi_y^2\,\mathrm{d}y}. \tag{A 5}$$

A wave of elevation or depression can be obtained depending on whether $\alpha_0 > 0$ or $\alpha_0 < 0$, respectively.

Returning to (A 2), a note on how this may be solved for the continuous profiles of $N^2(y)$ used in § 3 is now given. The solution for $\phi(y)$ may be written

$$\phi(y) = \sum_{n=0}^{n_y} a_n \sin(\gamma_n y), \tag{A 6}$$

for some (as yet) unknown a_n, with $\gamma_n = n\pi/L_y$. Here $n_y = 128$ typically. Cosine modes are eliminated due to the boundary conditions of the eigenproblem $\phi(0) = \phi(L_y) = 0$. Substituting (A 6) into (A 2), multiplying by $\sin(\gamma_m y)$ and integrating over the domain converts the problem into the standard matrix eigenvalue form $(\boldsymbol{A} - c_0^2\boldsymbol{I})\boldsymbol{b} = \boldsymbol{0}$, where $\boldsymbol{I}$ is the identity matrix and the elements of the matrix $\boldsymbol{A}$ and vector $\boldsymbol{b}$ are given by

$$A_{n,m} = \frac{2}{\gamma_n^2 L_y}\int_0^{L_y} N^2(y)\sin(\gamma_n y)\sin(\gamma_m y)\,\mathrm{d}y, \tag{A 7}$$

$$b_n = \gamma_n^2 a_n. \tag{A 8}$$

The eigenvectors and eigenvalues can be easily found using standard numerical methods (either LAPACK or NAG libraries for instance), giving a number of values for c_0 and $\boldsymbol{b}$ as eigenvalues and eigenvectors of the problem, respectively. The largest value of c_0 is associated with the vertical mode having no zeros except at the boundaries, and the required values of a_n can then easily be recovered from the associated b_n/γ_n^2.

REFERENCES

Aigner, A., Broutman, D. & Grimshaw, R. 1999 Numerical simulations of internal solitary waves with vortex cores. *Fluid Dyn. Res.* **25**, 315–333.

Benjamin, T. B. 1966 Internal waves of finite amplitude and permanent form. *J. Fluid Mech.* **25**, 241–270.

Benney, D. J. 1966 Long nonlinear waves in fluid flows. *J. Math. Phys.* **45**, 52–63.

Brown, D. J. & Christie, D. R. 1998 Fully nonlinear solitary waves in continuously stratified incompressible Boussinesq fluids. *Phys. Fluids* **10** (10), 2569–2586.

Carr, M., Fructus, D., Grue, J., Jensen, A. & Davies, P. A. 2008 Convectively induced shear instability in large-amplitude internal solitary waves. *Phys. Fluids* **20**, 12660.

Cheung, T. K. & Little, C. G. 1990 Meterological tower, microbarograph array, and sodar observations of solitary-like waves in the nocturnal boundary layer. *J. Atmos. Sci.* **47**, 2516–2536.

Choi, W. & Camassa, R. 1999 Fully nonlinear internal waves in a two-fluid system. *J. Fluid Mech.* **396**, 1–36.

Clarke, R. H., Smith, R. K. & Reid, D. G. 1981 The morning glory of the gulf of carpentaria: an atmospheric undular bore. *Mon. Weath. Rev.* **109**, 1726–1750.

Davis, R. E. & Acrivos, A. 1967 Solitary internal waves in deep water. *J. Fluid Mech.* **29** (3), 593–607.

Derzho, O. G. & Grimshaw, R. 1997 Solitary waves with a vortex core in a shallow layer of stratified fluid. *Phys. Fluids* **9**, 3378–3385.

Derzho, O. G. & Grimshaw, R. 2002 Solitary waves with recirculation zones in axisymmetric flows. *J. Fluid Mech.* **464**, 217–250.

Doviak, R. J., Chen, S. S. & Christie, D. R. 1991 A thunderstorm-generated solitary wave observation compared with theory for nonlinear waves in a sheared atmosphere. *J. Atmos. Sci.* **48**, 87–111.

Doviak, R. J. & Christie, D. R. 1989 Thunderstorm-generated solitary waves: a wind shear hazard. *J. Aircraft* **26**, 423.

Dritschel, D. G. 1995 A general theory for two-dimensional vortex interactions. *J. Fluid Mech.* **293**, 269–303.

Dritschel, D. G. & Ambaum, M. H. P. 1997 A contour-advective semi-lagrangian numerical algorithm for simulating fine-scale conservative dynamical fields. *Q. J. R. Meteorol. Soc.* **123**, 1097–1130.

Dritschel, D. G. & Fontane, J. 2010 The combined Lagrangian advection method. *J. Comput. Phys.* **229**, 5408–5417.

Dubreil-Jacotin, L. 1932 Sur les ondes type permantentes dans les liquides hétérogènes. *Atti dela Reale Academic Nationale dci Lincei* **15** (6), 44.

Fructus, D., Carr, M., Grue, J., Jensen, A. & Davies, P. A. 2009 Shear-induced breaking of large internal solitary waves. *J. Fluid Mech.* **620**, 1–29.

Fructus, D. & Grue, J. 2004 Fully nonlinear solitary waves in a layered stratified fluid. *J. Fluid Mech.* **505**, 323–347.

Funakoshi, M. & Oikawa, M. 1986 Long internal waves of large amplitude in a two-layer fluid. *J. Phys. Soc. Jpn.* **55** (1), 128–144.

Grimshaw, R. 1969 On steady recirculating flow. *J. Fluid Mech.* **39**, 695–703.

Grue, J., Jensen, A., Rusås, P.-O. & Sveen, J. K. 1999 Properties of large-amplitude internal waves. *J. Fluid Mech.* **380**, 257–278.

Grue, J., Jensen, A., Rusås, P.-O. & Sveen, J. K. 2000 Breaking and broadening of internal solitary waves. *J. Fluid Mech.* **413**, 181–217.

Helfrich, K. R. & Melville, W. K. 2006 Long nonlinear internal waves. *Annu. Rev. Fluid Mech.* **38**, 395–425.

Helfrich, K. R. & White, B. L. 2010 A model for large-amplitude internal solitary waves with trapped cores. *Nonlinear Process. Geophys.* **17**, 303–318.

Lamb, K. G. 2002 A numerical investigation of solitary internal waves with trapped cores formed via shoaling. *J. Fluid Mech.* **451**, 109–144.

Lamb, K. G. 2003 Shoaling solitary internal waves: on a criterion for the formation of waves with trapped cores. *J. Fluid Mech.* **478**, 81–100.

Lamb, K. G. 2008 On the calculation of the available potential energy of an isolated perturbation in a density-stratified fluid. *J. Fluid Mech.* **597**, 415–427.

Lamb, K. G. & Nguyen, V. T. 2009 Calculating energy flux in internal solitary waves with an application to reflectance. *J. Phys. Oceanogr.* **39**, 559–580.

Lamb, K. G. & Wan, B. 1998 Conjugate flows and flat solitary waves for a continuously stratified fluid. *Phys. Fluids* **10** (8), 2061–2079.

Long, R. R. 1953 Some aspects of the flow of stratified fluids. Part I. A theoretical investigation. *Tellus* **5**, 42–57.

Manasseh, R., Ching, C.-Y. & Fernando, H. J. S. 1998 The transition from density-driven to wave dominated isolated flows. *J. Fluid Mech.* **361**, 253–274.

Miles, J. W. 1961 On the stability of heterogeneous shear flows. *J. Fluid Mech.* **10**, 496–508.

Miles, J. W. 1980 Solitary waves. *Annu. Rev. Fluid Mech.* **12**, 11–43.

Moum, J. N., Farmer, D. M., Smyth, W. D., Armi, L. & Vagle, S. 2003 Structure and generation of turbulence at interfaces strained by internal solitary waves propagating shoreward over the continental shelf. *J. Phys. Oceanogr.* **33**, 2093–2112.

Ostrovsky, L. A. & Stepanyants, Y. A. 1989 Do internal solitons exist in the ocean? *Rev. Geophys.* **27**, 293–310.

Rusås, P.-O. & Grue, J. 2002 Solitary waves and conjugate flows in a three-layer fluid. *Eur. J. Mech.* B/*Fluids* **21**, 185–206.

Scotti, A. & Pineda, J. 2004 Observation of very large and steep internal waves of elevation near the massachusetts coast. *Geophys. Res. Lett.* **31**, L22307.

Stanton, T. P. & Ostrovsky, L. A. 1998 Observations of highly nonlinear internal solitons over the continental shelf. *Geophys. Res. Lett.* **25** (14), 2695–2698.

Stastna, M. & Lamb, K. G. 2002 Large fully nonlinear internal solitary waves: the effect of background current. *Phys. Fluids* **14** (9), 2987–2999.

Turkington, B., Eydeland, A. & Wang, S. 1991 A computational method for solitary internal waves in a continuously stratified fluid. *Stud. Appl. Maths* **85**, 93–127.

Vlasenko, V., Brandt, P. & Rubino, A. 2000 Structure of large-amplitude internal solitary waves. *J. Phys. Oceanogr.* **30**, 2172–2185.

White, B. L. & Helfrich, K. R. 2008 Gravity currents and internal waves in a stratified fluid. *J. Fluid Mech.* **616**, 327–356.

Yih, C.-S. 1960 Exact solutions for steady two-dimensional flow of a stratified fluid. *J. Fluid Mech.* **9**, 161–174.